Title

Quantitative PET reporter gene imaging of CD8+ T cells specific for a melanoma-expressed self-antigen.

Journal

International immunology, 21(2)

ISSN

0953-8178

Authors

Shu, Chengyi J
Radu, Caius G
Shelly, Stephanie M
et al.

Publication Date

2009-02-01

DOI

10.1093/intimm/dxn133

Peer reviewed

International Immunology, Vol. 21, No. 2, pp. 155–165
doi:10.1093/intimm/dxn133

Quantitative PET reporter gene imaging of CD8$^+$ T cells specific for a melanoma-expressed self-antigen

Chengyi J. Shu[1], Caius G. Radu[2,3], Stephanie M. Shelly[2], Dan D. Vo[4], Robert Prins[4,5], Antoni Ribas[5,6,7], Michael E. Phelps[2,3] and **Owen N. Witte[1,2,7,8]**

[1]Department of Microbiology, Immunology and Molecular Genetics, [2]Department of Molecular and Medical Pharmacology, [3]Crump Institute for Molecular Imaging, [4]Department of Surgery, [5]Jonsson Comprehensive Cancer Center, [6]Department of Medicine and [7]University of California at Los Angeles Eli and Edythe Broad Center of Regenerative Medicine and Stem Cell Research,
[8]Howard Hughes Medical Institute, University of California, Los Angeles, CA 90095-1662, USA

Keywords: cancer, immunotherapy, T lymphocytes

Abstract

Adoptive transfer (AT) T-cell therapy provides significant clinical benefits in patients with advanced melanoma. However, approaches to non-invasively visualize the persistence of transferred T cells are lacking. We examined whether positron emission tomography (PET) can monitor the distribution of self-antigen-specific T cells engineered to express an herpes simplex virus 1 thymidine kinase (*sr39tk*) PET reporter gene. Micro-PET imaging using the *sr39tk*-specific substrate 9-[4-[^{18}F]fluoro-3-(hydroxymethyl)-butyl]guanine ([^{18}F]FHBG) enabled the detection of transplanted T cells in secondary lymphoid organs of recipient mice over a 3-week period. Tumor responses could be predicted as early as 3 days following AT when a >25-fold increase of micro-PET signal in the spleen and 2-fold increase in lymph nodes (LNs) were observed in mice receiving combined immunotherapy versus control mice. The lower limit of detection was $\sim 7 \times 10^5$ T cells in the spleen and 1×10^4 T cells in LNs. Quantification of transplanted T cells in the tumor was hampered by the *sr39tk*-independent trapping of [^{18}F]FHBG within the tumor architecture. These data support the feasibility of using PET to visualize the expansion, homing and persistence of transferred T cells. PET may have significant clinical utility by providing the means to quantify anti-tumor T cells throughout the body and provide early correlates for treatment efficacy.

Introduction

Recent advances in tumor immunology have led to the development of novel immunotherapies for cancer. While clinical trials using cancer vaccines have yielded low objective response rates (1), recent approaches based on adoptive cell transfer immunotherapy have shown significantly higher efficacy. Rosenberg and colleagues have demonstrated partial and complete responses in ~50% of patients with metastatic melanoma treated with adoptive transfer (AT) of *ex vivo* expanded autologous tumor-infiltrating lymphocytes and a lymphodepleting host conditioning regime (2, 3). However, it remains unclear why some patients do not respond to treatment. Potential explanations include low TCR affinity for tumor antigens, sub-optimal *in vivo* expansion, failure of adoptively transferred T cells to gain access to secondary lymphoid organs or lack of tumor targeting. Currently, conventional immune monitoring approaches to address some of these potential rate-limiting steps involve quantitative and functional analyses of T cells isolated from peripheral blood or tumor biopsies (4). While these assays provide critical data, their main limitation stems from the inability to accurately reflect the dynamic changes in the distribution and numbers of T cells in lymphoid organs and at tumor sites. In particular, the potential for sampling error is increased in patients with metastatic disease and/or tumor lesions that are poorly accessible to surgical or fine needle biopsies. There is a need for non-invasive whole-body immune monitoring assays that correlate and/or predict the clinical endpoints of adoptive immunotherapy trials.

The advent of molecular imaging techniques could overcome these limitations by enabling serial and non-invasive visualization of adoptively transferred T cells throughout the body. Various techniques based on optical (5), nuclear (6) or magnetic resonance (7) imaging modalities have been used to visualize T cells *in vivo*. We and others have focused

Correspondence to: O. N. Witte; E-mail: owenw@microbio.ucla.edu

Received 10 June 2008, *accepted* 21 November 2008

Transmitting editor: J. P. Allison

Advance Access publication 23 December 2008

on developing positron emission tomography (PET) imaging approaches for immune monitoring [reviewed in (8)]. PET allows three-dimensional (3D) and quantitative measurements of the tissue accumulation of probes labeled with positron emitting radioisotopes. The sensitivity of PET is in the low nanomolar range and, unlike optical imaging modalities, measurements of probe accumulation are minimally impaired by tissue absorption and scattering. Importantly, PET studies in animal models are fully translatable to the clinic. Clinical PET scanners have similar sensitivities to micro-PET instruments used to image rodents. Furthermore, while their spatial resolution is a log order less than that of pre-clinical imaging systems, the physical size of the imaged human subject is also several orders of magnitude larger thereby reducing the resolution requirements.

A common thread among previous studies on PET imaging of anti-tumor T-cell responses relates to the strong immunogenicity of cancer antigens targeted in these studies (9–13). Using PET reporter gene imaging, Koehne *et al.* (9) visualized the accumulation of EBV-specific T cells in EBV-positive tumors expressing the correct HLA-restricting element but not in EBV-negative or HLA-mismatched tumors. In a series of studies, our group has demonstrated the capability of PET reporter gene imaging to monitor primary and secondary anti-tumor T-cell responses to xenoantigens encoded by sarcoma-inducing oncoretroviruses (10, 11, 13). Su *et al.* (14) established a correlation between the numbers of anti-tumor T cells specific for a model antigen and the retention of the reporter probe measured by PET. Similarly, another recent study correlated PET signal intensities over time with quantitation of transduced EBV-specific T cells detected in the tumor (15). While these studies have validated the feasibility of using PET reporter gene imaging for monitoring anti-tumor immunity, T-cell responses to strong foreign or model antigens are quantitatively different than those against non-mutated self-antigens more commonly expressed by human cancers of non-viral etiologies. In general, such autoreactive immune responses are of much lower magnitude than responses to foreign antigens and are mediated by low affinity T cells that have evaded central and peripheral tolerance induction mechanisms (16, 17). These differences raise the question whether PET reporter gene imaging has the required sensitivity to allow monitoring of T-cell responses against non-mutated self-antigens that are frequently targeted by adoptive immunotherapies in melanoma and other types of cancer (18).

In the current study, we used a model of adoptive immunotherapy against melanoma which reproduces several key aspects of the adoptive immunotherapy clinical trials performed at the National Cancer Institute (18, 19). To enable detection of T cells following AT, we transduced these cells with the PET reporter gene *sr39tk*, an optimized variant of the herpes simplex virus 1 (HSV1) thymidine kinase (20). Cells engineered to express *sr39tk* can be visualized by micro-PET using the high-affinity substrate (9-[4-[^{18}F]fluoro-3-(hydroxymethyl)-butyl]guanine ([^{18}F]FHBG) (21).

The findings of the current study were 3-fold: (i) the quantitation of T-cell expansion in lymphoid organs as measured by [^{18}F]FHBG micro-PET scans at early time points following AT was predictive of the efficacy of adoptive immunotherapy; (ii) *sr39tk*-expressing melanoma-specific T cells can be serially imaged by [^{18}F]FHBG micro-PET and (iii) the sensitivity of [^{18}F]FHBG PET reporter gene imaging enables detection of very low numbers of *sr39tk*+ T cells present in the spleen and lymph nodes (LNs) of treated mice. These data suggest that the ability of non-invasive PET imaging to measure the reconstitution, expansion and persistence of adoptively transferred T cells into patients may have significant clinical utility for providing early predictions of treatment efficacy. PET reporter imaging approaches can be incorporated into the design of clinical trials to evaluate novel adoptive T-cell-based immunotherapies against melanoma and other types of cancer.

Materials and methods

Cell lines and animals

B16-F10 (B16), a murine melanoma cell line, was obtained from the American Type Culture Collection (Rockville, MD, USA). Stably transfected cells were cultured in DMEM (Gibco BRL, Gaithersburg, MD, USA) supplemented with 10% FCS (Gemini, Calabasas, CA, USA). C57BL/6 and pmel-1 mice were bred and maintained according to the guidelines of the Department of Laboratory Animal Medicine (DLAM) at the University of California, Los Angeles. All animal studies were carried out by using protocols that had been approved by DLAM.

In vitro activation of pmel-1 T cells and retroviral transduction

The retroviral vector of murine stem cell virus (pMSCV) (22) containing a 5′ long terminal repeat-driven truncated version of the *sr39tk* fused with super enhanced yellow fluorescent protein (*seYFP*) was used to generate high-titer helper-free retrovirus stocks prepared by transient co-transfection of 293T cells. LNs were harvested from pmel-1 mice and cultured with IL-2 (100 U ml^{-1}) and gp100$_{25–33}$ peptide (1 μg ml^{-1}). At 48 and 72 h post-activation, the cells were spinfection with the MSCV-*sr39tk-seYFP* retrovirus (~10 multiplicity of infection) and 2 μg ml^{-1} of lipofectamine (1800 r.p.m., 120 min, 32°C, Beckman CS-6R centrifuge). Upon *in vitro* stimulation, pmel-1 CD8$^+$ T cells developed an early effector phenotype defined by activation markers such as up-regulation of CD25 and CD69 and of lymphoid-homing molecules (partial down-regulation of CD62L and expression of CCR7) (23). Approximately >95% of all of the adoptively transferred cells were CD8$^+$/Vβ13+ T cells (data not shown). *seYFP* was used to monitor transduction efficiency before AT, which was routinely >50–70%.

AT, vaccination and tumor treatment

Six- to 12-week old female C57BL/6 were injected subcutaneously (s.c.) with 1 × 10^5 B16 melanoma cells on day −8. On day −1, lymphopenia was induced by sub-lethal irradiation (500 cGy) of tumor-bearing mice. On the next day (day 0), mice with similarly sized tumors were randomized into groups: (i) no adoptive cell transfer therapy (ATX), (ii) ATX of 2–5 × 10^6 transduced pmel-1 cells and (iii) ATX of 2–5 × 10^6 transduced pmel-1 cells plus gp100$_{25–33}$ peptide-pulsed dendritic cell (DC) and human IL-2 (50 000 IU intra-peritoneally for 3 days after each DC administration). Caliper measurements of the tumors were recorded, and the tumor volume was calculated with the formula: 4/3π × width radius × length radius × height radius.

DC preparation

DCs were differentiated from bone marrow progenitor cells obtained from C57BL/6 mice by *in vitro* culture in murine granulocyte macrophage colony-stimulating factor (100 ng ml^{-1}; Amgen, Thousand Oaks, CA, USA) and murine IL-4 (500 U ml^{-1}; R&D Systems, Minneapolis, MN, USA) as described by Inaba (24), with minor modifications (25). DCs were harvested as loosely adherent cells, washed twice in PBS (Mediatech, Herndon, VA, USA) and pulsed with $gp100_{25–33}$ peptide at a concentration of 10 μM in serum-free media for 90 min at room temperature. Each mouse received $\sim 10^6$ pulsed DCs given s.c. at 4 sites on the back.

Micro-PET/computed tomography imaging

Animals were anesthetized, injected intravenously (i.v.) with [^{18}F]FHBG and scanned using a FOCUS 220 micro-PET scanner (Siemens, Knoxville, TN, USA) as described previously (20). Images were reconstructed from the scanner data by using an iterative maximum *a posteriori* algorithm (26). In the same session, mice were injected i.v. with Fenestra LC contrast agent (Advanced Research Technologies, Quebec, Canada) and computed tomography (CT) images were acquired on a micro-CAT II instrument (Siemens). Using Amide, quantification was performed by drawing regions of interest (ROIs) to determine the amount of [^{18} F]FHBG (microcurie) present. Animals were euthanized on approximately day 3 post-AT, immediately following micro-PET imaging. Spleen, LNs and tumors were harvested, scanned by micro-PET *ex vivo* and then counted in a gamma counter (Perkin Elmer).

Isolation and analysis of adoptively transferred cells

Single-cell suspensions were prepared by dissociating LNs through a mesh cell strainer in DMEM + 5% fetal bovine serum media. Single-cell suspensions of spleens were prepared in media containing 1.5 mg type IV DNase (Roche, Mannheim, Germany). RBCs were lysed with 1× PharmLyse buffer (PharMingen, San Diego, CA, USA). Tumors were dissected, minced and incubated at 37°C for 1–2 h in media containing 1.5 mg type IV DNase, 15 mg type IV collagenase (Gibco) and 37.5 U type V hyaluronidase (Sigma, St Louis, MO, USA). Ficoll gradients were performed on single-cell suspensions. Cells were mixed with a known number of Accucount Blank Particles (Spherotech, Libertyville, IL, USA), stained with 7AAD (Becton Dickinson) and analyzed on a FACSCanto instrument (Becton Dickinson). Total cell density and viability were calculated from the ratio of 7AAD to beads using the Diva software (BD). Cells were also stained with Vβ13-FITC (BD) and CD8–PE–Cy7 (BD) to determine the percentage of Vβ13+ *sr39tk-seYFP*+ CD8 T cells. Linear regressions of the total number of Vβ13+ *sr39tk*+ cells versus the amount of [^{18}F]FHBG (microcurie) present in tissues of interest were analyzed using the PRISM software (version 4.02; GraphPad, San Diego, CA, USA).

Autoradiography and histology

Mice were anesthetized with 2% isoflurane and injected i.v. with 500 μCi of [^{18}F]FHBG. After 1 h, mice were sacrificed and tumors were harvested and embedded in the optimum cutting temperature compound (Sakura Finetek, Torrance, CA, USA). Frozen sections (4 μm) were sliced using a microtome (Leica) and exposed on BAS-TR2025 imaging screens overnight (FujiFilm Life Science, Stamford, CT, USA). The screens were developed a BAS-5000 phosphor imager (Fuji-Film Life Science). Hematoxylin and eosin staining was performed on the same frozen sections.

Results

[^{18}F]FHBG PET/CT imaging enables visualization of melanoma-specific CD8$^+$ T cells in the spleen and LNs of tumor-bearing mice

Pmel-1 TCR transgenic mice were used to determine whether T-cell responses specific for tumor-expressed self-antigens can be visualized by PET reporter gene imaging. CD8$^+$ T cells from these mice express a TCR specific for an antigenic epitope derived from the unmutated melanoma/melanocyte-associated antigen, gp100. Tumor regression requires a combined immunotherapy protocol consisting of AT of T cells, lymphodepletion (X-ray therapy, XRT), peptide-pulsed DC vaccination and high-dose systemic IL-2 (full regime, Fig. 1A) (19, 23, 27, 28). Omission of any of these components compromises treatment efficacy and results in tumor progression. In a series of four independent studies, we confirmed the requirement for $gp100_{25–33}$/DC and IL-2 to induce regression of established B16 melanoma following AT of pmel-1 cells (Fig. 1B).

Ex vivo-stimulated pmel-1 T cells were retrovirally transduced with the PET reporter gene *sr39tk* to enable visualization and tracking with PET imaging (Fig. 1A). [^{18}F]FHBG micro-PET images were merged with high spatial resolution CT images to provide anatomical information. High-definition whole-body mouse images were generated by algebraic reconstruction of collected 3D emission data (26). 3D PET images are displayed as a measure of percent injected dose per gram of tissue in a false color scale, with red indicating the highest amount of radioactivity present at that location. In mice, [^{18}F]FHBG also accumulates non-specifically in the gall bladder, small and large intestine as well as in the kidney and bladder due to clearance of the non-phosphorylated probe by hepatobiliary and renal routes. To overcome the background in the lower abdomen, a contrast agent (Fenestra LC) was used for precise identification of the spleen using micro-CT imaging.

Mice were imaged on day 3 post-transfer. Top panels of Fig. 2 show representative 3D whole-body [^{18}F]FHBG micro-PET/CT scans of mice receiving the full regime (XRT + AT + IL-2 + DC) or incomplete therapy (XRT + AT). We focused on three anatomical locations: spleen, LNs and the tumor. [^{18}F]FHBG signals corresponding to the spleen were observed in mice receiving the full regime, the only therapy leading to objective tumor responses (Fig. 1A). The [^{18}F]FHBG spleen signal was reproducibly observed in all scanned animals from the full regime group (N = 37, eight independent experiments). Eight-six percentage of mice receiving the full regime also showed [^{18}F]FHBG accumulation in peripheral LNs (PLNs), including the axillary, brachial and cervical nodes (Fig. 2A, bottom panel). In contrast, none of the mice receiving AT and lymphodepletion without

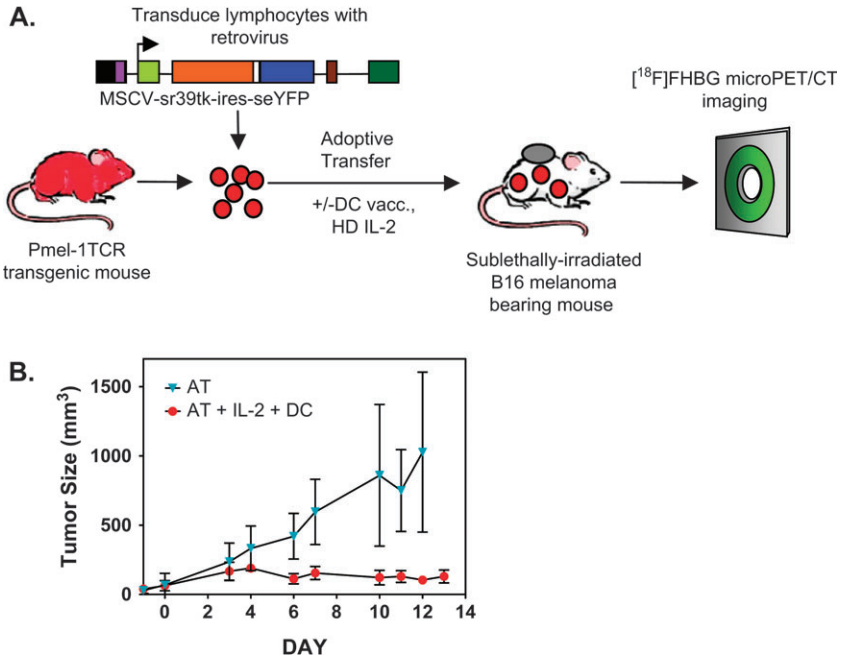

Fig. 1. Experimental design to evaluate PET reporter gene imaging in a clinically relevant model of cancer immunotherapy. C57BL/6 mice were implanted s.c. with 1×10^5 B16 melanoma cells in the right shoulder on day −8. Mice underwent a lymphodepleting regimen on day −1. The following day, mice received an AT of $\sim 5 \times 10^6$ pmel-1 T cells genetically labeled with a retroviral vector co-expressing HSV1-*sr39tk* and seYFP. One group of mice received additional $gp100_{25–33}$/DC vaccination and high-dose IL-2 treatment. [^{18}F]FHBG micro-PET imaging was performed on different days. (A) General schematic. (B) Tumor volume measurement over time in the group of mice receiving pmel-1 cells' AT alone (XRT + AT) and pmel-1 cells with $gp100_{25–33}$/DC vaccine and high-dose IL-2 (XRT + AT + IL-2 + DC).

vaccination and cytokine treatment (XRT + AT group, $N = 30$, in seven independent experiments) showed detectable [^{18}F]FHBG accumulation in secondary lymphoid organs (Fig. 2B, bottom panel). Therefore, at this early time point (72 h post-transfer), [^{18}F]FHBG micro-PET/CT detected T-cell homing and expansion at the spleen and LNs. Quantitation of [^{18}F]FHBG retention in secondary lymphoid organs allowed us to non-invasively differentiate between mice with and without combined immunotherapy.

Non-specific accumulation of [^{18}F]FHBG at the tumor site

As shown in the bottom panels of Fig. 2, both groups of mice receiving full regime or incomplete therapy showed detectable accumulation of [^{18}F]FHBG in the B16 melanoma lesions. We reasoned that such signals could be explained by two potential mechanisms. First, adoptively transferred *sr39tk*+ T cells could traffic to the tumor independently of the DC vaccination and IL-2 treatment. Second, the signal at the tumor site could reflect *sr39tk*+ T-cell-independent trapping of the probe. When tumors of mice receiving AT of *sr39tk*+ T cells with and without full regime were dissociated, the number of Vβ13+ *sr39tk*+ cells present did not correlate with the [^{18}F]FHBG signal measured (Fig. 3A and B). To further distinguish between these two possibilities, B16 tumor-bearing mice that received only whole-body irradiation without AT of *sr39tk*+ T cells (the XRT group) were imaged. As shown in Fig. 2(C), we observed non-specific accumulation of [^{18}F]FHBG in the B16 tumors from the XRT-treated group. Tumor sizes measured with calipers correlated with [^{18}F]FHBG retention quantified by 3D ROIs drawn around the tumor (Fig. 3C and D). These data suggest that the [^{18}F]FHBG signals observed at the tumor site likely reflect an *sr39tk*+ T-cell-independent mechanism.

We reason that four possible mechanisms could account for the [^{18}F]FHBG accumulation in B16 tumors: (i) [^{18}F]FHBG is retained in B16 cells by a transport mechanism and/or enzymatic modification or slow efflux out of the cells; (ii) [^{18}F]FHBG is phosphorylated by an endogenous kinase expressed in B16 cells; (iii) [^{18}F]FHBG is incorporated in the DNA of B16 cells and (iv) the abnormal vasculature of B16 tumors could decrease [^{18}F]FHBG clearance through a 'blood pooling' effect. To investigate these possibilities, we performed *in vitro* and *in vivo* experiments. Pro-B cell lines (Ba/F3) engineered to stably express *sr39tk* were used as positive controls. *In vitro*, B16 cells did not retain or phosphorylate [^{18}F]FHBG after 1 h incubation (Supplementary Figure 1A and B, available at *International Immunology* Online). Unlike *sr39tk*+ Ba/F3 and pmel T cells, which incorporated [^{18}F]FHBG into the DNA after 4 h, DNA incorporation of [^{18}F]FHBG was undetectable in B16 cells (Supplementary Figure 1C, available at *International Immunology* Online). Mice bearing B16 and Ba/F3-*sr39tk* tumors were injected with [^{18}F]FHBG and 1 h later mice were sacrificed to isolate tumor cells. In contrast to Ba/F3-*sr39tk* tumors, there was no detectable retention, phosphorylation or DNA incorporation of [^{18}F]FHBG in the B16, *sr39tk*-negative tumors (Supplementary Figure 1D–F, available at *International Immunology* Online). Non-specific probe trapping could also be

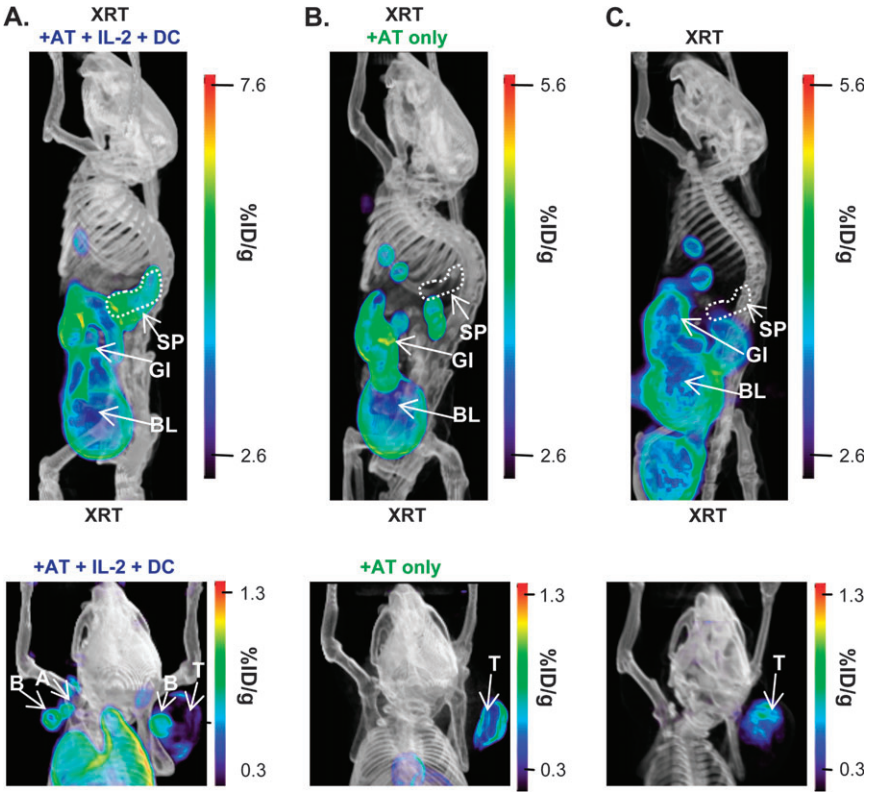

Fig. 2. [^{18}F]FHBG micro-PET imaging of adoptively transferred T cells in spleen and LNs in mice receiving combined immunotherapy. On day 3 post-AT, mice were imaged with micro-PET/CT 60 min after i.v. injection with [^{18}F]FHBG and Fenestra LC contrast agent. Representative 3D PET/CT images of lymphodepleted mice bearing B16 tumors receiving (A) pmel-1 T cells with gp100$_{25–33}$/DC vaccine and high-dose IL-2 (XRT + AT + IL-2 + DC), (B) pmel-1 T cells alone (XRT + AT) and (C) no treatment (XRT only) showing the whole body (top panels) and upper body (bottom panels) are presented. %ID/g, percent injected dose per gram of tissue; SP, spleen; GI, gastrointestinal tract; BL, bladder; B, brachial LN; A, axillary LN; T, tumor; GB, gall bladder; E, eye.

explained by the particular architecture of the B16 tumors. These tumors are highly vascularized and show areas of blood pooling which could decrease probe clearance, as shown by histology and autoradiography (Fig. 3E). Given these observations, in subsequent experiments, we focused on imaging T cells in secondary lymphoid organs which, in contrast to B16 lesions, do not show non-specific retention of [^{18}F]FHBG.

[^{18}F]FHBG micro-PET/CT serial imaging detects changes in the persistence and trafficking of adoptively transferred T cells

Eight mice treated with the full regime were serially imaged by [^{18}F]FHBG micro-PET between days 1 and 21 post-AT. As shown in Fig. 4(A), these mice received three doses of gp100$_{25–33}$/DC vaccination and systemic IL-2 treatment at 6-day intervals (red arrows, Fig. 4B) (27). The micro-PET imaging schedule was selected based on previous studies showing that maximal expansion of adoptively transferred pmel-1 T cells in recipient mice can be detected on days 5–7 post-AT in the spleen, tumor draining LNs (DLNs) and at the tumor site (29). Later time points were included to determine if repeated DC vaccination and IL-2 treatment could induce micro-PET measurable changes in the distribution and/or numbers of adoptively transferred T cells.

Following the rapid expansion of adoptively transferred cells visualized in the spleen on day 3 post-transfer (Fig. 2A), the [^{18}F]FHBG signal at this site showed a slight decrease on day 5 (data not shown). No [^{18}F]FHBG micro-PET spleen signals could be detected after day 8 (data not shown). These dynamic changes in the splenic [^{18}F]FHBG retention could reflect the rapid initial expansion of adoptively transferred cells due to homeostatic proliferation in a lymphodepleted environment with an exogenous supply of IL-2 and/or the antigen-dependent T-cell proliferation by gp100-pulsed DCs, followed by the contraction phase at later time points (29). Alternatively, the loss of the [^{18}F]FHBG spleen signal after day 8 could indicate the homing of the *sr39tk*+ T cells to LNs, the tumor site and other organs. Accordingly, starting on day 3 post-transfer, six out of eight mice showed significant [^{18}F]FHBG accumulation in several LN groups including axillary, brachial and cervical (Fig. 4B and Supplementary Figure 2, available at *International Immunology* Online). In the remaining two mice, detection of [^{18}F]FHBG signals at PLNs was delayed until day 5 (Supplementary Figure 2, available at *International Immunology* Online). In contrast to the spleen signal, the accumulation of [^{18}F]FHBG in LN groups was

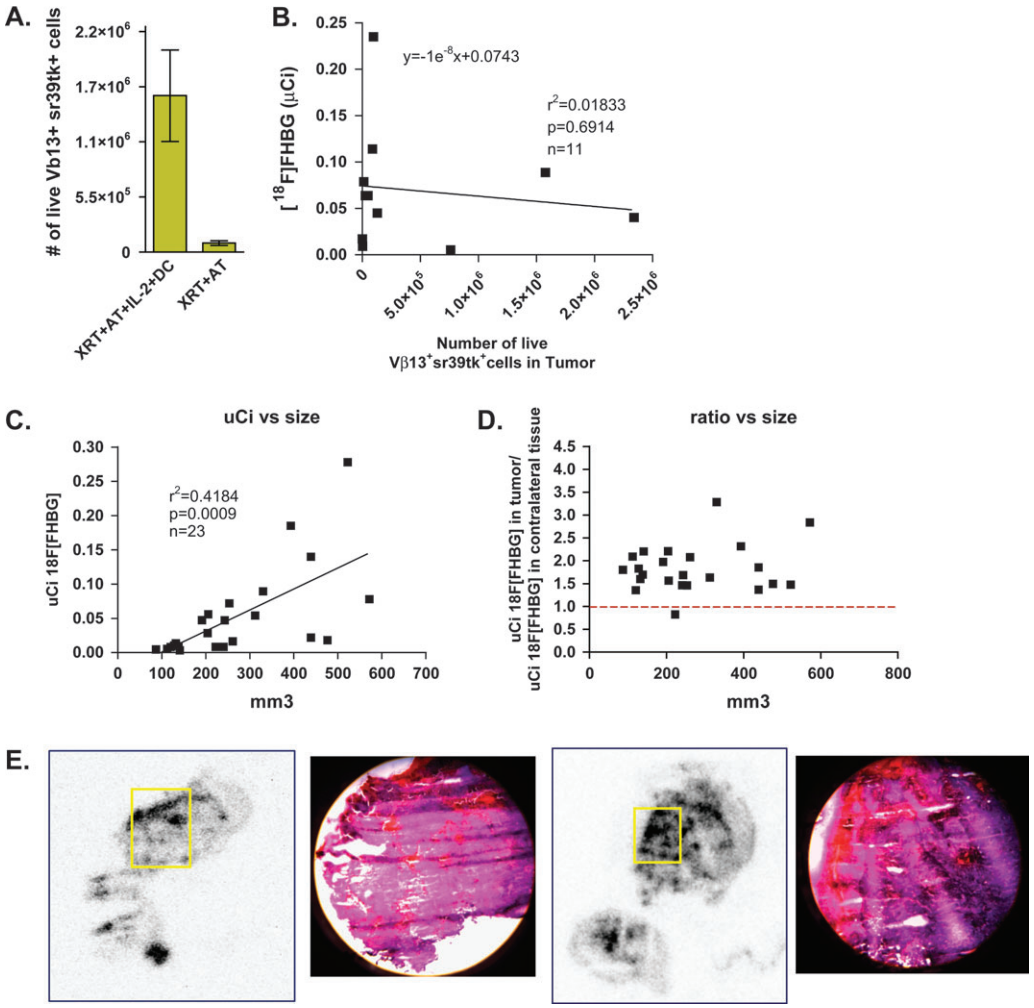

Fig. 3. Non-specific [^{18}F]FHBG accumulation and trapping in B16 tumors. (A) Tumors from the XRT + AT + IL-2 + DC and XRT + AT group were isolated, the accumulated [^{18}F]FHBG radioactivity counted with the gamma counter and the cells were analyzed by FACS. (B) Correlation of *in vivo* [^{18}F]FHBG retention with the number of Vβ13+ *sr39tk*+ cells present in tumor. (C) Lymphodepleted mice bearing different B16 tumor masses without AT of *sr39tk* transduced pmel-1 T cells were imaged with [^{18}F]FHBG micro-PET. Correlation of *in vivo* [^{18}F]FHBG retention at the tumor with B16 tumor size. (D) Ratio of *in vivo* [^{18}F]FHBG uptake at the tumor site versus a contralateral background region plotted against B16 tumor size suggest that the [^{18}F]FHBG accumulation is independent of the presence of *sr39tk*+ cells. (E) Autoradiography and histology suggest that areas of [^{18}F]FHBG accumulation correspond to blood pools in the tumor.

more sustained and could be detected beyond day 8, until day 19. It is important to note that the patterns of [^{18}F]FHBG accumulation in LNs were highly variable between individual mice (Supplementary Figure 2, available at *International Immunology* Online). Furthermore, we did not observe higher [^{18}F]FHBG accumulation in tumor DLNs relative to contralateral LNs. This finding could indicate that the homing/expansion of *sr39tk*+ T cells in PLNs reflects systemic effects of the DC vaccination and IL-2 treatment rather than priming of these cells in tumor DLNs by tumor-derived antigens.

Quantification of [^{18}F]FHBG PET signals in secondary lymphoid organs

The experimental strategy shown in Fig. 5(A) was used to determine whether the numbers of adoptively transferred *sr39tk*+ T cells in the spleen and LNs of treated mice correlate with [^{18}F]FHBG accumulation measured *in vivo* by micro-PET. Immediately following whole-body micro-PET scans, mice receiving the full regime or XRT + AT were sacrificed and isolated organs were imaged by micro-PET *ex vivo*. As shown in Fig. 5(B), *ex vivo* scans confirmed the identity of the lymphoid organs imaged *in vivo*. Gamma counter measurements were performed to more precisely estimate the [^{18}F]FHBG retention in isolated organs. We observed increased amounts of [^{18}F]FHBG in the spleens of mice receiving the full regime (1.9 ± 0.4 μCi) versus XRT + AT-treated mice (0.05 ± 0.01 μCi, $P < 0.05$). The same pattern was detected in LNs isolated from these mice (23.0 ± 4.6 nCi for the full regime-treated mice versus 3.3 ± 0.9 nCi for XRT + AT-treated mice, $P < 0.05$). The *in vivo* micro-PET ROI-based measurements of [^{18}F]FHBG retention showed an excellent correlation with radioactivity measurements of *ex vivo* lymphoid organs acquired by the gamma counter, thus confirming our method to quantify the [^{18}F]FHBG micro-PET signals (data not shown).

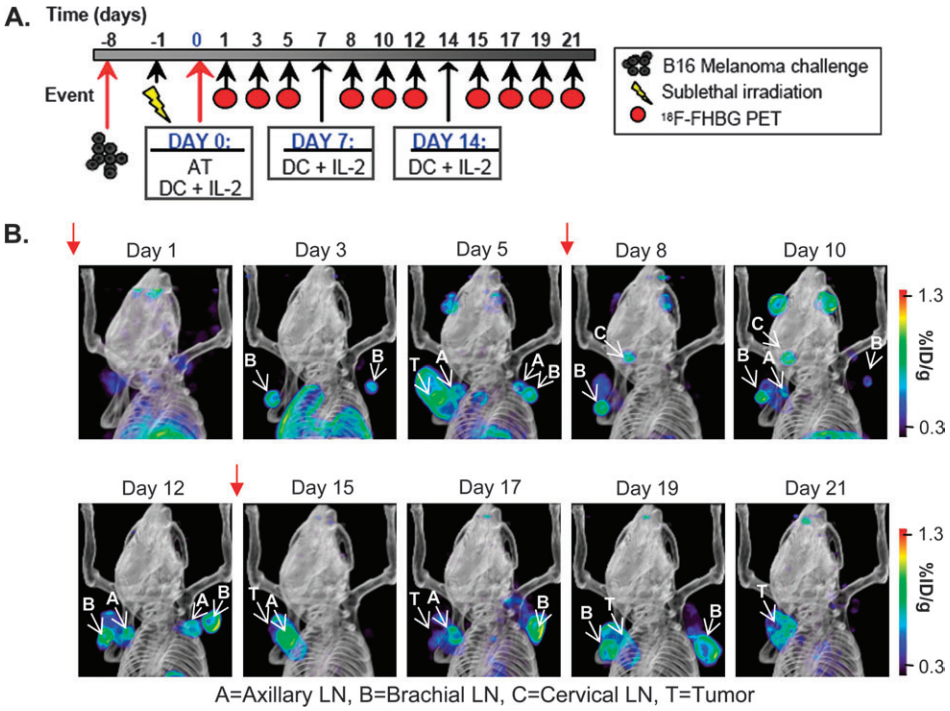

Fig. 4. Serial [^{18}F]FHBG micro-PET imaging of T-cell persistence at various anatomical locations in mice treated with combined immunotherapy. (A) Time line of the imaging study. (B) Mice were imaged with micro-PET/CT 60 min after i.v. injection with [^{18}F]FHBG. Representative 3D micro-PET/CT images of the same mouse on different days are displayed. Red arrows indicate days that mice received gp100$_{25–33}$/DC vaccine and high-dose IL-2. A, axillary LN; B, brachial LN; C, cervical LN; T, tumor.

To determine whether the numbers of Vβ13+ *sr39tk*+ pmel-1 T cells present in secondary lymphoid organs correlate with the amount of [^{18}F]FHBG detected at these sites, we performed flow cytometric analyses on single-cell suspensions isolated from spleen and LNs. We observed higher percentages and total numbers of *sr39tk*+ cells expressing the Vβ13+ pmel-1 TCR in the spleens and LNs of mice treated with the full regime compared with the XRT + AT group (Fig. 5C). ROI-based quantitation of *in vivo* [^{18}F]FHBG accumulation in the spleen and LNs showed a good correlation with numbers of Vβ13+ *sr39tk*+ cells present (Fig. 5D and E). Linear regression analysis of spleen signals predicted the accumulation of ~60 nCi of [^{18}F]FHBG per 10^6 cells in a 22 mm^3 volume (Fig. 5D). For LNs, these numbers were ~12.8 nCi of [^{18}F]FHBG per 10^5 cells in a 2–3 mm^3 volume (Fig. 5E).

Discussion

Advantages and limitations of PET reporter gene imaging of adoptive immunotherapy in cancer

Adoptive immunotherapies aim to overcome immunological tolerance to cancer by transferring autologous tumor-specific T cells expanded *ex vivo*. Although promising 'proof-of-concept' studies have been reported in recent years, identification of suitable biomarkers of protective T-cell anti-tumor immune responses remains a major challenge. We describe a PET reporter gene imaging approach which allows visualization of melanoma-specific T cells following AT in tumor-bearing mice. The advantages of this approach are as follows: (i) the ability to sequentially monitor adoptive immunotherapy for extended periods of time; (ii) high sensitivity, as demonstrated by the capability to detect rare populations of T cells at various anatomical locations and (iii) the safety, pharmacokinetics and dosimetry of [^{18}F]FHBG have been studied in rats, rabbits and normal human volunteers, and the US Food and Drug Administration has approved its use as an investigational new drug in clinical trials (30–32). These studies simplify the regulatory steps required to translate this imaging approach from mice to cancer patients. [^{18}F]FHBG PET imaging of adenovirally introduced *HSV1-tk* into tumors of patients with hepatocellular cancer has been demonstrated (33, 34). Another advantage of this approach is that *HSV1-tk* was originally designed for suicide gene therapy of cancer. Thus, *HSV1-tk* would be delivered to cancer cells and then administration of a pharmacological dose of gancyclovir would cause death of these cells. This built-in safety feature should prevent possible adverse effects, including malignant transformation as a consequence of random insertion of viral constructs and life-threatening autoimmunity. The combination of [^{18}F]FHBG and *HSV1-sr39tk* can also be used for monitoring the distribution of stem cells and the effects of suicide gene therapy in clinical trials.

Several clinical trials showed that HSV1-tk gene-modified lymphocytes for allogeneic hematopoietic stem cell transplants in leukemic patients could be detected in circulation, bone marrow and peripheral tissues for >12 months, while maintaining their anti-tumor activity (35–38). However, using quantitative PCR assays, these studies have also revealed a significant

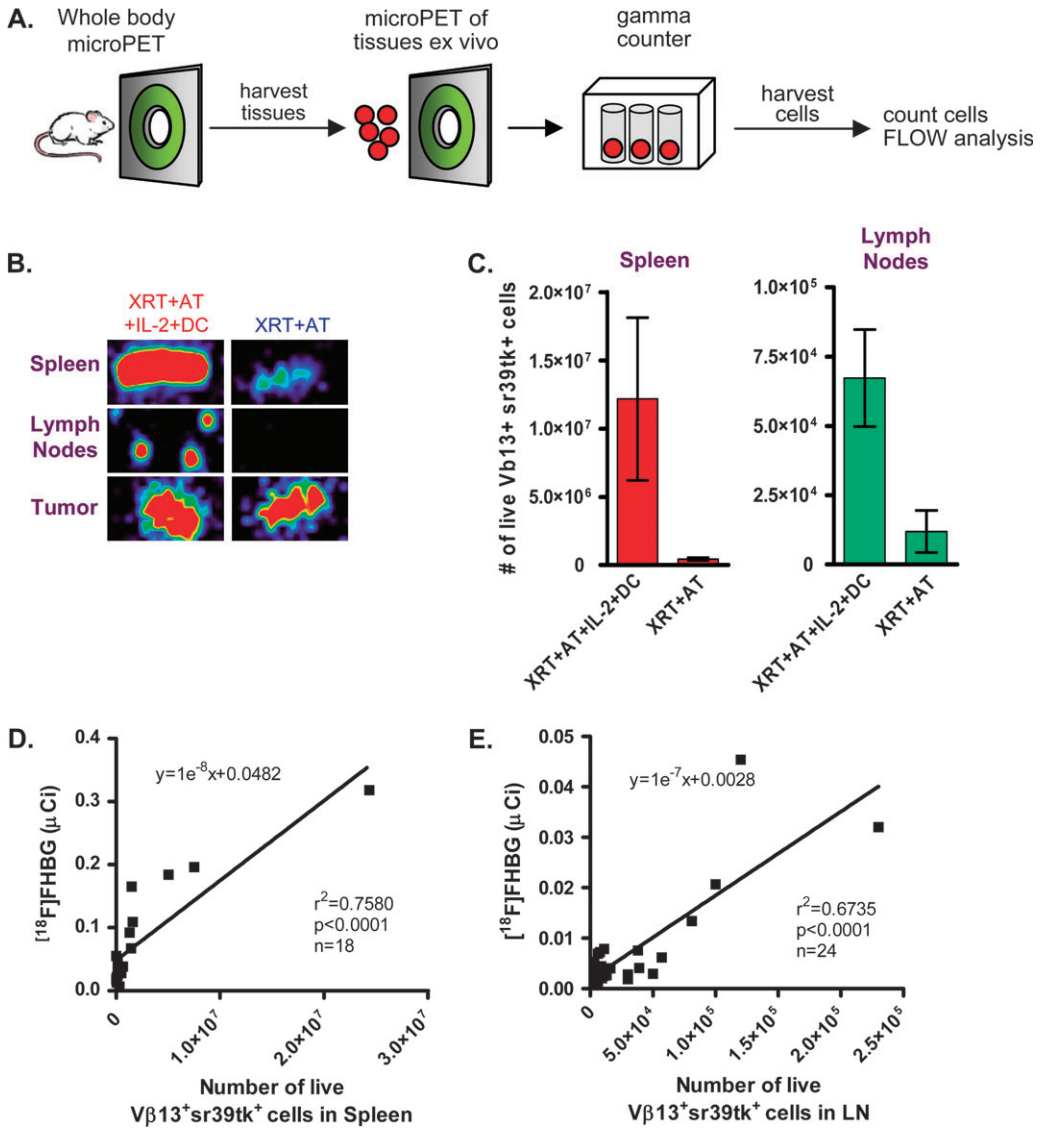

Fig. 5. *Ex vivo* correlation of [^{18}F]FHBG retention with numbers of Vβ13+ *sr39tk*+ cells present in the spleen and LNs. (A) General schematic. Mice were injected i.v. with [^{18}F]FHBG on day 3 post-AT. Immediately after whole-body imaging, spleen and LNs were isolated, (B) imaged *ex vivo* by micro-PET, counted with the gamma counter and cells were analyzed by FACS. Mice receiving partial treatment (XRT + AT) and combined immunotherapy group (XRT + AT + IL-2 + DC) were compared. (C) Increased numbers of live Vβ13+ *sr39tk*+ T cells in the organs of mice from the combined immunotherapy group (XRT + AT + IL-2 + DC) compared with the XRT + AT group. Correlation of *in vivo* [^{18}F]FHBG retention with the numbers of Vβ13+ *sr39tk*+ cells present in (D) spleen and (E) LNs.

incidence (in ~23% of patients) of immune responses against HSV1-tk, leading to a decrease in the number of circulating cells (35, 39). In contrast, it is possible that the myeloablative chemotherapeutic regime will significantly reduce the possibility of host immune responses against *sr39tk*+ adoptively transferred T cells. Other options to approach the immunogenicity problem are to (i) use less immunogenic HSV1-*sr39tk* variants (40) or (ii) develop alternative non-immunogenic PET reporter genes. In this context, a recent study by Ponomarev *et al.* (41) proposed the use of the human thymidine kinase 2 as a potentially non-immunogenic PET reporter gene. The human norepinephrine transporter (hNET) has been recently evaluated as a potentially non-immunogenic PET reporter gene. Using the norepinephrine analog ^{124}I-MIBG, Doubrovin *et al.* (15) showed that as few as 10^4 T lymphocytes transduced *ex vivo* with an hNET construct could be visualized by micro-PET *in vivo*. The investigators used this approach to monitor tumor infiltration by antigen-specific T lymphocytes. The availability of ^{18}F-labeled hNET substrates could widen the applicability of this approach for monitoring cell-based therapies (15). The development of novel PET probed specific for immune cells could enable direct imaging of immune responses and therefore circumvent the use of PET reporter genes. We have recently developed 1-(2′-deoxy-2′-^{18}F-fluoroarabino-furanosyl) cytosine ([^{18}F]FAC), a novel PET imaging probe (42). [^{18}F]FAC enabled visualization of lymphoid organs such as thymus, spleen and LNs by micro-PET. The probe was useful for imaging localized immune activation in a mouse model of anti-tumor immunity and enabled detection of changes in lymphoid mass in systemic autoimmunity.

Another potential limitation of *sr39tk* PET reporter imaging is the non-specific accumulation of the *sr39tk* substrate [^{18}F]FHBG in B16 melanoma lesions. This could complicate the visualization of adoptively transferred T cells in the target tissue. It is currently unclear whether the [^{18}F]FHBG background at the tumor site represents a more general problem or an experimental artifact specific to the B16 melanoma. We found that the architecture of these B16 tumor lesions includes areas of relatively large blood pools which may cause non-specific probe trapping. In contrast to other tumors in which [^{18}F]FHBG slowly clears from the tumors after 2–3 h, the probe did not clear from B16 tumors during this time frame (data not shown). Moreover, our data showed that the trapping of [^{18}F]FHBG is correlated with the size of the tumor. This finding complicated our experiments because these tumors quickly reach >1 cm in diameter 1–2 weeks after injection of as few as 1×10^5 melanoma cells. The non-specific retention of [^{18}F]FHBG has not been observed in other tumors studied by our group and others [i.e. retroviral induced rhabdomyosarcoma and EL4 tumors (11, 13)]. A study by Penuelas *et al.* (34) allowed visualization of adenoviral-mediated transgene expression in the liver tumors of patients after the initial non-specific accumulation of [^{18}F]FHBG by hepatocytes was cleared through the gall bladder.

The issue of potential non-specific [^{18}F]FHBG accumulation in human cancers still needs to be addressed. If such non-specific [^{18}F]FHBG signals are observed, then baseline PET scans prior to adoptive therapy might be required. The [^{18}F]FHBG 'background' may be relatively constant since tumors in patients do not grow as rapidly as the B16 tumors. To further demonstrate the feasibility of this imaging approach, we have imaged mice with large tumors (>1 cm diameter) before and after intratumoral injections of pmel-*sr39tk* T cells. The [^{18}F]FHBG signal in the tumor following T-cell injection increased by 3- to 5-fold (Supplementary Figure 3, available at *International Immunology* Online). Nonetheless, our findings indicate the need to further optimize existing PET reporter gene approaches by (i) development of PET reporter genes that are less immunogenic and potentially more sensitive than *sr39tk* and (ii) radiochemical synthesis and testing of novel *sr39tk* substrates with lower non-specific accumulation than FHBG.

The lower limit of detection of PET reporter gene imaging

The approach described here was sensitive to variations in the strength of the immunotherapeutic regime and allowed quantitative measurements of [^{18}F]FHBG accumulation in the spleen and LNs of treated mice. These measurements correlated well with the numbers of *sr39tk*+ melanoma-specific T cells present at these sites determined *ex vivo* using flow cytometry. We observed that the lower limit of detection, defined as the lowest number of *sr39tk*+ T cells detected by micro-PET, was dependent on the anatomical location of these cells. In the spleen, the lower limit of detection was $\sim 7 \times 10^5$ *sr39tk*+ T cells or in terms of accumulated radioactivity, ~55 nCi of [^{18}F]FHBG. To enable detection by micro-PET, at least ~10% of the total number of cells in the spleen had to express the *sr39tk* reporter. In contrast, the limit of detection in LNs was 1×10^4 *sr39tk*+ cells, corresponding to ~2–5 nCi of [^{18}F]FHBG, or a frequency of at least ~3% of the total number of cells. The apparent discrepancy between sensitivity parameters in spleen and LNs could be explained by the different architecture of these secondary lymphoid organs. Unlike LNs that consist mainly of lymphocytes, spleens contain a red pulp compartment populated by macrophages and erythrocytes and few lymphocytes. Our data indicate a density of white blood cells in the spleen of $\sim 0.8 \times 10^5$ mm^{-3} compared with $\sim 3 \times 10^5$ mm^{-3} in a LN.

When clinical PET scanners are used to image the heart, brain or tumors, signals from tissues of interest are typically 1.5- to 10-fold above background levels. Our data are within this dynamic range. For example, although PET signal from the brain striatum is typically ~3-fold over background levels in healthy individuals, the precision of PET allows clinicians to monitor the loss of dopaminergic neurons in Parkinson patients (43).

While our results indicate that PET reporter gene imaging has sufficient sensitivity to enable repeated and non-invasive monitoring of adoptive immunotherapy in a clinically relevant animal model, further improvements might be necessary to fully achieve the potential of this approach. The limit of detection of small animal PET scanners is related to both their sensitivity as well as their intrinsic noise characteristics (44). While our studies used the micro-PET Focus 220 system (3.5% sensitivity), new instruments such as the Inveon micro-PET (Siemens) are expected to have three times larger peak sensitivity (~10%), from purely geometrical considerations. Furthermore, methods to reduce the intrinsic noise that stems from the natural radioactivity background of the tomographs have been developed (45). Both these factors (increased sensitivity and energy windowing) can be applied simultaneously to acquisitions that are approaching the limit of detection. It is therefore likely that future studies will enable imaging of a much lower number of cells than those shown here. It is important to note that the lower limit of detection is essentially the same throughout the mouse body (surface or deep), in contrast to bioluminescence or other optical imaging modalities. Similar improvements to enhance sensitivity and resolution are also being performed on clinical PET scanners.

PET imaging biomarkers to evaluate adoptive immunotherapies

A critical finding of our work was that no reproducible patterns of [^{18}F]FHBG accumulation in different LNs across different time points and animals could be observed. While this finding likely reflects the inherent individual variability of T-cell responses and the need for longitudinal immune monitoring studies at a whole-body level, it also raises the question of how PET reporter gene imaging can assist the development of predictive biomarkers. Furthermore, our data emphasize the utility of using reporter gene imaging to non-invasively follow and further understand the variability of distribution and expansion of adoptively transferred T cells in lymphoid organs of patients. Concerning the B16 melanoma model, we observed that the most informative scans were those performed at early time points following AT. Thus, mice showing at least 2-fold increase of [^{18}F]FHBG retention in the spleen and LNs rejected the B16 tumors, whereas the lack of PET probe accumulation at these sites correlated

with tumor progression. Importantly, while [^{18}F]FHBG micro-PET scans at later time points (up to 3 weeks) still showed a similar correlation, the treatment efficacy was easily assessed after day 5 by simply measuring the tumor volumes using calipers or CT imaging. Future studies are required to determine whether our findings regarding the optimal schedule of PET reporter gene imaging for defining predictive biomarkers can be generalized to other models of adoptive immunotherapy.

In conclusion, PET reporter gene imaging of AT of melanoma-specific T cells can be used to study the *in vivo* dynamics of AT of tumor antigen-specific T cells and to define non-invasive predictive biomarkers of treatment efficacy. This technique is amenable to clinical translation and could be incorporated in the next generation of clinical trials to evaluate novel immunotherapy approaches in melanoma and potentially other malignancies.

Supplementary data

Supplementary figures are available at *International Immunology* Online.

Funding

Dana Foundation; Merck Research Laboratories to C.G.R.; Fred Eiserling and Judith Lengyel Graduate Doctorate Fellowship to C.J.S.; US Department of Energy Contract (DE-FG02-06ER64249) to M.E.P.; National Cancer Institute Grant (R24CA92865).

Acknowledgements

We are grateful to W. Ladno and J. Edwards for PET imaging, Satyamurthy and cyclotron group for production of [^{18}F]FHBG. We thank G. Toy, M. Riedinger, S. Quan, D. Chen and A. Tran for outstanding technical assistance. We also thank B. Anderson for help with preparing the manuscript. O.N.W. is an Investigator of the Howard Hughes Medical Institute.

Abbreviations

AT	adoptive transfer
ATX	adoptive transfer treatment
CT	computed tomography
3D	three-dimensional
DC	dendritic cell
DLAM	Department of Laboratory Animal Medicine
DLN	draining LN
[^{18}F]FAC	1-(2′-deoxy-2′-^{18}F-fluoroarabino-furanosyl) cytosine
[^{18}F]FHBG	9-[4-[^{18}F]fluoro-3-(hydroxymethyl)butyl]guanine
hNET	human norepinephrine transporter
HSV1	herpes simplex virus 1; i.v., intravenously
LN	lymph node
MSCV	murine stem cell virus
PET	positron emission tomography
PLN	peripheral LN
ROI	region of interest
seYFP	super enhanced yellow fluorescent protein
sr39tk	HSV1 thymidine kinase; s.c., subcutaneously
XRT	X-ray therapy

References

1 Rosenberg, S. A., Yang, J. C. and Restifo, N. P. 2004. Cancer immunotherapy: moving beyond current vaccines. *Nat. Med.* 10:909.
2 Dudley, M. E., Wunderlich, J. R., Robbins, P. F. *et al.* 2002. Cancer regression and autoimmunity in patients after clonal repopulation with antitumor lymphocytes. *Science* 298:850.
3 Dudley, M. E., Wunderlich, J. R., Yang, J. C. *et al.* 2005. Adoptive cell transfer therapy following non-myeloablative but lymphodepleting chemotherapy for the treatment of patients with refractory metastatic melanoma. *J. Clin. Oncol.* 23:2346.
4 Comin-Anduix, B., Gualberto, A., Glaspy, J. A. *et al.* 2006. Definition of an immunologic response using the major histocompatibility complex tetramer and enzyme-linked immunospot assays. *Clin. Cancer Res.* 12:107.
5 Negrin, R. S. and Contag, C. H. 2006. *In vivo* imaging using bioluminescence: a tool for probing graft-versus-host disease. *Nat. Rev. Immunol.* 6:484.
6 Serganova, I. and Blasberg, R. 2005. Reporter gene imaging: potential impact on therapy. *Nucl. Med. Biol.* 32:763.
7 Pittet, M. J., Swirski, F. K., Reynolds, F., Josephson, L. and Weissleder, R. 2006. Labeling of immune cells for *in vivo* imaging using magnetofluorescent nanoparticles. *Nat. Protoc.* 1:73.
8 Hildebrandt, I. J. and Gambhir, S. S. 2004. Molecular imaging applications for immunology. *Clin. Immunol.* 111:210.
9 Koehne, G., Doubrovin, M., Doubrovina, E. *et al.* 2003. Serial *in vivo* imaging of the targeted migration of human HSV-TK-transduced antigen-specific lymphocytes. *Nat. Biotechnol.* 21:405.
10 Dubey, P., Su, H., Adonai, N. *et al.* 2003. Quantitative imaging of the T cell antitumor response by positron-emission tomography. *Proc. Natl Acad. Sci. USA* 100:1232.
11 Su, H., Chang, D. S., Gambhir, S. S. and Braun, J. 2006. Monitoring the antitumor response of naive and memory CD8 T cells in RAG1-/- mice by positron-emission tomography. *J. Immunol.* 176:4459.
12 Ponomarev, V., Doubrovin, M., Lyddane, C. *et al.* 2001. Imaging TCR-dependent NFAT-mediated T-cell activation with positron emission tomography *in vivo*. *Neoplasia* 3:480.
13 Shu, C. J., Guo, S., Kim, Y. J. *et al.* 2005. Visualization of a primary anti-tumor immune response by positron emission tomography. *Proc. Natl Acad. Sci. USA* 102:17412.
14 Su, H., Forbes, A., Gambhir, S. S. and Braun, J. 2004. Quantitation of cell number by a positron emission tomography reporter gene strategy. *Mol. Imaging Biol.* 6:139.
15 Doubrovin, M. M., Doubrovina, E. S., Zanzonico, P., Sadelain, M., Larson, S. M. and O'Reilly, R. J. 2007. *In vivo* imaging and quantitation of adoptively transferred human antigen-specific T cells transduced to express a human norepinephrine transporter gene. *Cancer Res.* 67:11959.
16 Pardoll, D. M. 1999. Inducing autoimmune disease to treat cancer. *Proc. Natl Acad. Sci. USA* 96:5340.
17 Gattinoni, L., Powell, D. J. Jr, Rosenberg, S. A. and Restifo, N. P. 2006. Adoptive immunotherapy for cancer: building on success. *Nat. Rev. Immunol.* 6:383.
18 Dudley, M. E. and Rosenberg, S. A. 2003. Adoptive-cell-transfer therapy for the treatment of patients with cancer. *Nat. Rev. Cancer* 3:666.
19 Overwijk, W. W., Theoret, M. R., Finkelstein, S. E. *et al.* 2003. Tumor regression and autoimmunity after reversal of a functionally tolerant state of self-reactive CD8+ T cells. *J. Exp. Med.* 198:569.
20 Gambhir, S. S., Bauer, E., Black, M. E. *et al.* 2000. A mutant herpes simplex virus type 1 thymidine kinase reporter gene shows improved sensitivity for imaging reporter gene expression with positron emission tomography. *Proc. Natl Acad. Sci. USA* 97:2785.
21 Yaghoubi, S. S., Wu, L., Liang, Q. *et al.* 2001. Direct correlation between positron emission tomographic images of two reporter genes delivered by two distinct adenoviral vectors. *Gene Ther.* 8:1072.
22 Hawley, R. G., Lieu, F. H., Fong, A. Z. and Hawley, T. S. 1994. Versatile retroviral vectors for potential use in gene therapy. *Gene Ther.* 1:136.
23 Gattinoni, L., Klebanoff, C. A., Palmer, D. C. *et al.* 2005. Acquisition of full effector function *in vitro* paradoxically impairs the *in vivo* antitumor efficacy of adoptively transferred CD8+ T cells. *J. Clin. Invest.* 115:1616.
24 Inaba, K., Inaba, M., Romani, N. *et al.* 1992. Generation of large numbers of dendritic cells from mouse bone marrow cultures supplemented with granulocyte/macrophage colony-stimulating factor. *J. Exp. Med.* 176:1693.

25 Ribas, A., Butterfield, L. H., McBride, W. H. *et al.* 1997. Genetic immunization for the melanoma antigen MART-1/Melan-A using recombinant adenovirus-transduced murine dendritic cells. *Cancer Res.* 57:2865.
26 Qi, J., Leahy, R. M., Cherry, S. R., Chatziioannou, A. and Farquhar, T. H. 1998. High-resolution 3D Bayesian image reconstruction using the microPET small-animal scanner. *Phys. Med. Biol.* 43:1001.
27 Lou, Y., Wang, G., Lizee, G. *et al.* 2004. Dendritic cells strongly boost the antitumor activity of adoptively transferred T cells *in vivo*. *Cancer Res.* 64:6783.
28 Antony, P. A., Piccirillo, C. A., Akpinarli, A. *et al.* 2005. CD8+ T cell immunity against a tumor/self-antigen is augmented by CD4+ T helper cells and hindered by naturally occurring T regulatory cells. *J. Immunol.* 174:2591.
29 Palmer, D. C., Balasubramaniam, S., Hanada, K. *et al.* 2004. Vaccine-stimulated, adoptively transferred CD8+ T cells traffic indiscriminately and ubiquitously while mediating specific tumor destruction. *J. Immunol.* 173:7209.
30 Yaghoubi, S., Barrio, J. R., Dahlbom, M. *et al.* 2001. Human pharmacokinetic and dosimetry studies of [(18)F]FHBG: a reporter probe for imaging herpes simplex virus type-1 thymidine kinase reporter gene expression. *J. Nucl. Med.* 42:1225.
31 Yaghoubi, S. S., Couto, M. A., Chen, C. C. *et al.* 2006. Preclinical safety evaluation of 18F-FHBG: a PET reporter probe for imaging herpes simplex virus type 1 thymidine kinase (HSV1-tk) or mutant HSV1-sr39tk's expression. *J. Nucl. Med.* 47:706.
32 Yaghoubi, S. S. and Gambhir, S. S. 2006. PET imaging of herpes simplex virus type 1 thymidine kinase (HSV1-tk) or mutant HSV1-sr39tk reporter gene expression in mice and humans using [18F]FHBG. *Nat. Protoc.* 1:3069.
33 Penuelas, I., Haberkorn, U., Yaghoubi, S. and Gambhir, S. S. 2005. Gene therapy imaging in patients for oncological applications. *Eur. J. Nucl. Med. Mol. Imaging* 32 (Suppl 2):S384.
34 Penuelas, I., Mazzolini, G., Boan, J. F. *et al.* 2005. Positron emission tomography imaging of adenoviral-mediated transgene expression in liver cancer patients. *Gastroenterology* 128:1787.
35 Bonini, C., Ferrari, G., Verzeletti, S. *et al.* 1997. HSV-TK gene transfer into donor lymphocytes for control of allogeneic graft-versus-leukemia. *Science* 276:1719.
36 Tiberghien, P., Ferrand, C., Lioure, B. *et al.* 2001. Administration of herpes simplex-thymidine kinase-expressing donor T cells with a T-cell-depleted allogeneic marrow graft. *Blood* 97:63.
37 Riddell, S. R., Elliott, M., Lewinsohn, D. A. *et al.* 1996. T-cell mediated rejection of gene-modified HIV-specific cytotoxic T lymphocytes in HIV-infected patients. *Nat. Med.* 2:216.
38 Berger, C., Flowers, M. E., Warren, E. H. and Riddell, S. R. 2006. Analysis of transgene-specific immune responses that limit the *in vivo* persistence of adoptively transferred HSV-TK-modified donor T cells after allogeneic hematopoietic cell transplantation. *Blood* 107:2294.
39 Verzeletti, S., Bonini, C., Marktel, S. *et al.* 1998. Herpes simplex virus thymidine kinase gene transfer for controlled graft-versus-host disease and graft-versus-leukemia: clinical follow-up and improved new vectors. *Hum. Gene Ther.* 9:2243.
40 Ossevoort, M., Zaldumbide, A., Cramer, S. J., van der Voort, E. I., Toes, R. E. and Hoeben, R. C. 2006. Characterization of an immuno 'stealth' derivative of the herpes simplex virus thymidine-kinase gene. *Cancer Gene Ther.* 13:584.
41 Ponomarev, V., Doubrovin, M., Shavrin, A. *et al.* 2007. A human-derived reporter gene for noninvasive imaging in humans: mitochondrial thymidine kinase type 2. *J. Nucl. Med.* 48:819.
42 Radu, C. G., Shu, C. J., Nair-Gill, E. *et al.* 2008. Molecular imaging of lymphoid organs and immune activation by positron emission tomography with a new [(18)F]-labeled 2′-deoxycytidine analog. *Nat. Med.* 14:783.
43 Morrish, P. K., Sawle, G. V. and Brooks, D. J. 1996. An [18F]dopa-PET and clinical study of the rate of progression in Parkinson's disease. *Brain* 119(Pt 2):585.
44 Goertzen, A. L., Suk, J. Y. and Thompson, C. J. 2007. Imaging of weak-source distributions in LSO-based small-animal PET scanners. *J. Nucl. Med.* 48:1692.
45 Currie, L. A. 1968. Limits for qualitative detection and quantitative determination—application to radiochemistry. *Anal. Chem.* 40:586.